Materials Science & Engineering A 642 (2015) 1–6

Contents lists available at ScienceDirect

Materials Science & Engineering A

journal homepage: www.elsevier.com/locate/msea

Fabrication of high-strength graphene nanosheets/Cu composites by accumulative roll bonding

Xueran Liu [a,b], Dajie Wei [b], Limin Zhuang [b], Can Cai [b], Yonghao Zhao [b,*]

[a] School of Materials Engineering, Yancheng Institute of Technology, Yancheng 224051, Jiangsu, China
[b] Nanostructural Materials Research Center, School of Materials Science and Engineering, Nanjing University of Science and Engineering, Nanjing 210094, Jiangsu, China

ARTICLE INFO

Article history:
Received 19 March 2015
Received in revised form
4 June 2015
Accepted 9 June 2015
Available online 11 June 2015

Keywords:
Graphene nanosheets/Cu composites
Accumulative roll bonding
Microstructure
Mechanical properties

ABSTRACT

Graphene nanosheets (GNSs) reinforced copper matrix composites have been considered as the potential copper materials with high strength and high conductivity. Here, the high-strength GNSs/Cu composites were fabricated by accumulative roll bonding (ARB). The ARBed GNSs/Cu composites manifested a good interfacial bonding and a significant grain refinement. The average spacing of high-angle boundaries along the normal direction was less than 150 nm after 6 ARB cycles, which was finer than that of the ARBed Cu. In addition, there existed a nano-layer with grain sizes of 50–70 nm and the high-density deformation-twins at the interface. The tensile strength of the ARBed materials enhanced with the number of cycles. After six cycles, the tensile strength of GNSs/Cu composites reached 496 MPa. This strength was 275 and 33 MPa higher than those of the annealed copper and the ARBed copper, respectively due to the strain hardening and grain refinement. Furthermore, the addition of GNSs into Cu matrix accelerated the grain refinement and the strength improvement.

1. Introduction

Explosive development in machinery, electronic and rail transit industries highly requires copper matrix composites that possess high strength and excellent thermal and electrical properties. Previous studies [1–3] have demonstrated that the strength and wear resistance can be significantly enhanced by introducing second phase (ceramic particles, carbon fiber, carbon nanocube, etc) into the Cu matrix. Also, by using graphene, which has unique physical, chemical and mechanical properties, as the reinforcement, one could also improve the mechanical properties of copper matrix composites [4–6]. For example, for a 1.0 wt% graphene nanosheets (GNSs) reinforced Al6061 fabricated by hot compaction, flexural strength is enhanced by 47% as compared to the Al6061 counterpart [7]. The Mg–Al alloy reinforced with 0.6 wt% graphene nanoplatelets (GNPs) exhibits improvements in 0.2% yield strength, ultimate tensile and failure strain [8]. Moreover, bulk 1.0 vol% GNS–Ni/Cu composites fabricated by spark plasma sintering show a 94% increase in yield strength [9]. Nevertheless, the GNSs tend to tangle and agglomerate into clusters, mainly due to the van der Waals interactions between aromatic rings [10]. Up to now very limited studied have been focused on the graphene/metal composite materials, because of the difficulty of dispersion and interfacial bonding.

Several reported methods to fabricate GNSs/metal composites are ball milling or ultrasonic dispersion, and then followed by sintering, casting, or electrodeposition [7–9,11–14]. However, these processes cannot effectively solve the dispersion problem of GNSs in the metal matrix. Notably, the poor dispersion of GNSs in the metal matrix directly affects the mechanical and electronic properties of the GNSs/metal composites. By using the rolling process, Sruti [15] and Kim [16] prepared the GNSs/metal composites with extremely uniform microstructure and high electrical conductivity. In their method [15], graphene oxide was spread on the In and In–Ga alloy foils, then the composite foils were repeatedly processed by folding and rolling. Kim et al. [16] used ball milling and high-ratio differential speed rolling (HRDSR) to fabricate multi-layer graphene (MLG) reinforced Cu matrix composites. The strength of MLG/Cu composites was enhanced due to the increased dispersion of the MLGs. In this regard, rolling process is believed to be an effective method to obtain the graphene/metal composites with a uniform microstructure. More recently, several researchers used accumulative roll bonding (ARB) process for fabrication particles reinforced metal matrix composites (MMCs), such as SiC/Al MMCs [17,18], Al_2O_3/Al MMCs [19,20], Cu_p/Al MMCs [21], Al_2O_3/Cu MMCs [22], SiC/Cu MMCs [23], and SiC/IF steel [24]. Dispersion of reinforcements in metal matrix and mechanical properties of MMCs has been remarkably improved after ARB

* Corresponding author. Fax: +86 2584315304.
E-mail address: yhzhao@mail.njust.edu.cn (Y. Zhao).

http://dx.doi.org/10.1016/j.msea.2015.06.032
0921-5093/

process. Therefore, one would expect that the ARB process could manufacture GNSs reinforced Cu matrix composites.

In this work, we performed the ARB process to fabricate uniformly dispersed, ultrafine-grained (UFG) and high-strength GNSs/Cu composites. We focused on the microstructure and mechanical properties of the ARBed GNSs/Cu composites. We then studied the effects of GNSs on the grain refinement and strengthening in comparison with the ARBed pure Cu, and found that the addition of GNSs into Cu matrix accelerated the grain refinement and the strength improvement. In addition, we discussed the strengthening mechanism of the ARBed GNSs/Cu composites.

2. Experimental procedures

2.1. ARB process

Oxygen free copper sheets were cut into 150 mm × 25 mm × 1 mm strips and annealed in the vacuum furnace at 773 K for 2 h to obtain coarse state. The original surface roughness of the strips was about Ra=0.58 μm along both the rolling direction (RD) and the transverse direction (TD). The surfaces of upper and lower strips were firstly degreased by acetone and brushed with a rotating steel brush. After scratch brushing, the surface roughness was about Ra=2.80 μm. The clean and fresh surface is exceedingly important for a good interfacial bonding. GNSs with a dimension of less than about 10 nm × 15 μm were used as the reinforcement, and were uniformly dispersed in acetone by ultrasonic device for 2 h. The suspension was then sprayed using an airbrush on the surface of the copper strip. The amount of GNSs was about 0.05 mg/mm^2. Finally two strips were stacked together, fastened by steel wire and rolled without lubrication by means of a rolling mill with a loading capacity of 20 tons. The reduction in thickness was nominally 50% and the roll speed was 0.34 m/s per rolling cycle. After the first rolling cycle, the rolled specimens were cut into two halves, and the same procedures of adding GNSs and subsequent rolling were repeated once to finish the second ARB cycle. The above procedure proceeded up to eight ARB cycles without adding any GNSs. In order to identify the GNSs effects, the same copper strips were ARBed up to eight cycles without GNSs were also prepared.

2.2. Investigations of microstructure and mechanical properties

The morphology of GNSs was characterized by transmission electron microscopy (TEM) in a FEI Tecnai 20 device operating at 200 kV. Fourier transform infrared spectroscopy (FTIR) spectrum was measured in a TENSOR 27 device. The RD–ND planes of ARBed specimens were mechanically polished and then electropolished in a solution of phosphoric acid and deionized water (17:3 by volume). The microstructures of ARBed specimens were analyzed by scanning electron microscopy (SEM) in a FEI Quanta 250F device operating at 20 kV and transmission electron microscopy (TEM) in a FEI Tecnai 20 device operating at 200 kV. Tensile test was performed using a W+b tensile machine at an initial strain rate of $5.6 \times 10^{-4}\,s^{-1}$ at room temperature. Tensile specimens were 15 mm and 2 mm in gage length and gage width, respectively. Tensile fracture surfaces were observed by SEM.

3. Results and discussion

3.1. Microstructure

Fig. 1 shows a typical FTIR spectrum of the graphene nanosheets. The most characteristic feature of graphene nanosheet is broad, and the bands of stretching vibration appear at 1734, 1576 and 1219 cm^{-1}, respectively. Inset of the figure illustrates a typical TEM image of the graphene nanosheets. Graphene nanosheets are a crumpled and folded structure with the thickness of less than 10 nm.

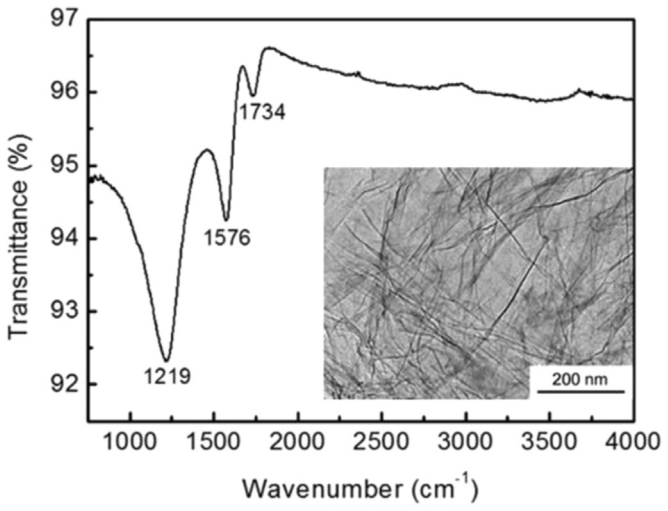

Fig. 1. FTIR spectrum of the GNSs. Inset is a TEM image of the GNSs.

Fig. 2 shows the microstructures of GNSs/Cu composites ARBed for different cycles at the RD–ND plane. Graphene nanosheets (white color) exist between copper layers, and the bonded interfaces can be clearly seen between layers. A few parts of unbonded interfaces with cavities can be found near graphene nanosheets (see Fig. 2a and b). With increasing the number of ARB cycles, the dispersion of graphene nanosheets changes more and more uniformly in copper matrix and the unbounded interface becomes less and less. After eight ARB cycles, it is difficult to identify the bonded interfaces and porosities in the GNSs/Cu composites (see Fig. 2d).

Fig. 3a and b shows TEM micrographs of the copper without GNSs and GNSs/Cu composites ARBed for 6 cycles at the RD–ND plane, respectively. The equivalent strain is 4.8, suggesting that the ultrafine lamellar boundary structure is formed by ARB along the rolling direction in both Cu and GNSs/Cu composites. For the ARBed Cu, the average spacing of high-angle boundaries along the normal direction is about 200–300 nm (see Fig. 3a). However, for the ARBed GNSs/Cu composites, the average spacing of lamellar grains along the normal direction is about 100–150 nm, being much smaller than the ARBed Cu. For both samples, a large number of dislocation lines and dislocation webs can be clearly observed within the ultrafine lamellar grains. A lot of dislocations aggregate towards grain boundaries or other local regions. The above result indicates that the presence of the graphene nanosheets leads to more grain refinement during ARB process. The same grain refinement phenomena have also been found in the particle reinforced metal matrix in the ARB process [17–22]. Moreover, for the GNSs/Cu composites ARBed for 8 cycles, we observe a nano-layer at the copper–copper bonding interface which has a thickness of about 300 nm and a grain size of 50–70 nm, as shown in Fig. 3c. In addition, deformation-twins (marked by white arrows) are also frequently observed near the interface.

The TEM micrograph of GNSs/Cu composites ARBed for 6 cycles is shown in Fig. 4. Bright interface zone is the graphene nanosheet (see the selected area diffraction pattern), which exhibits a good interfacial bonding between Cu and graphene nanosheet. In addition, Cu nano-twins with misorientation angle of approximate 45° are found near graphene nanosheet.

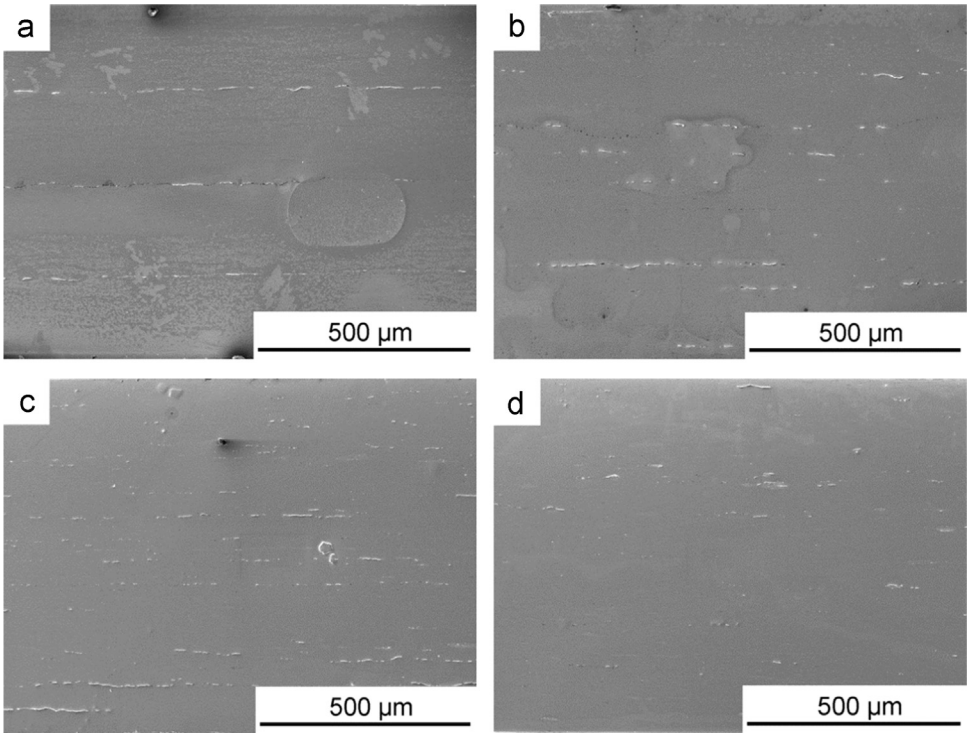

Fig. 2. SEM microstructures of the GNSs/Cu composites ARBed for: (a) 2 cycles, (b) 4 cycles, (c) 6 cycles, and (d) 8 cycles.

ARB process availably improves the dispersion of GNSs in the Cu matrix, as shown in Fig. 2. The improvement of reinforcements distribution in the matrix was previously reported in the SiC, Al_2O_3, or nano-sized SiO_2 reinforced aluminum composites fabricated by ARB [17,25,26]. Alizadeh found that the distribution of SiC particles in the Al matrix became more and more homogeneous with the increase in ARB cycles [17]. The length of the specimen doubles its original one after a ARB deformation, which results in the increase of particles dispersion in the matrix. In addition, ARB deformation can also enhance the interfacial bonding between GNS and Cu, as shown in Fig. 4. After 6 ARB cycles, the obvious porosities are not observed in the interface between GNS and Cu. The interfacial bonding can be improved by further plastic deformation and the newest interface is the weakest in the ARB process [26]. Furthermore, a host of geometrically necessary dislocations are introduced by a large amount of shear strain during ARB, which results in the formation of UFG ranging from 100 nm to 300 nm [27]. However, the significant effect of GNSs on the grain refinement has been confirmed by TEM analysis in this study. Addition of GNSs into Cu is especially susceptible to the formation of more UFGs and even NCs by ARB. Obviously, copper–graphene interfaces play the more crucial role in restricting the

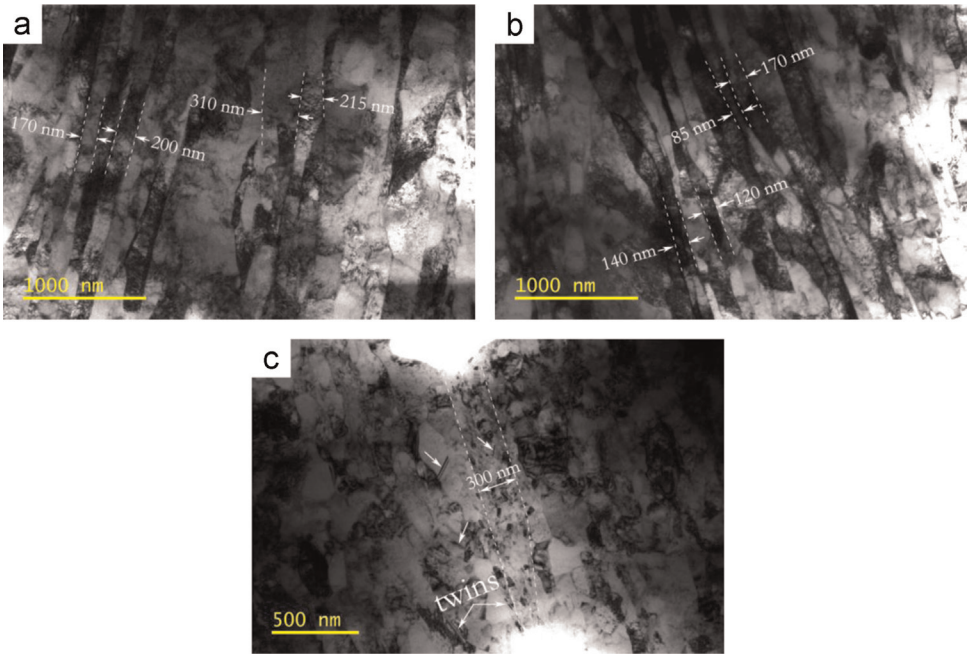

Fig. 3. TEM micrographs of the Cu ARBed for 6 cycles (a), the GNSs/Cu composites ARBed for 6 cycles (b) and 8 cycles (c).

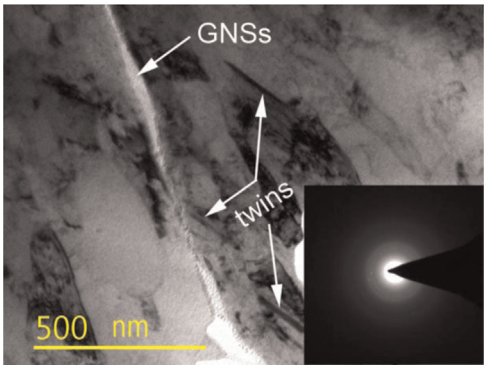

Fig. 4. TEM micrograph of the GNSs/Cu composites ARBed for 6 cycles. Inset is a selected diffraction pattern of GNSs.

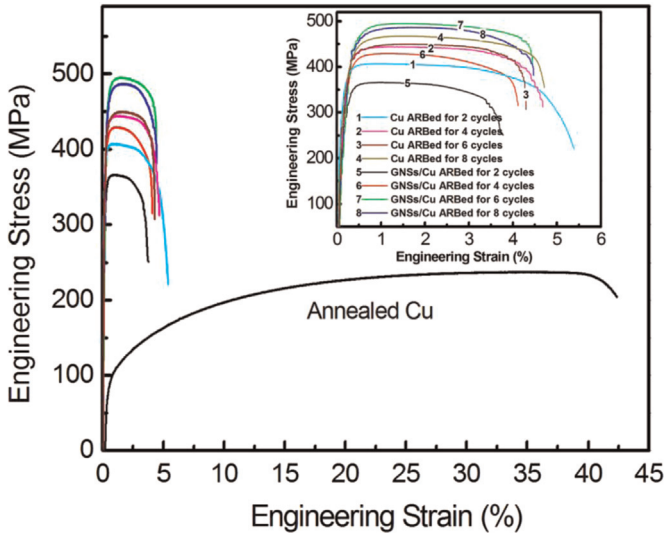

Fig. 5. Engineering stress–strain curves of Cu and GNSs/Cu composites ARBed for different cycles. Inset is the magnification.

dislocation motion than copper–copper interfaces. In general, carbonaceous materials and copper show non-wetting behavior and non-solid solubility at the ambient temperature [28,29]. Therefore, chemical reactions between GNSs and Cu matrix cannot occur during ARB. There are typical dislocation cells insisting of a multitude of sub-boundaries and Cu nanotwins near interface in the GNSs/Cu ARBed for 6 cycles, as shown in Figs. 3b and 4. GNSs restrain the interfacial bonding between copper and copper, which leads to the difficulty of dislocation motion and stress concentration at the interface. Hence, the increase in the deformation-twin density is found at the interface between GNSs and Cu. It indicates that ARB deformation mechanism is controlled by dislocation motion and twin deformation.

3.2. Mechanical properties

3.2.1. Tensile properties

Fig. 5 shows engineering stress–strain curves of Cu and GNSs/Cu composites ARBed for different cycles. The effects of ARB process on the tensile properties of copper and GNSs/Cu composites are obvious. The tensile strength of UFG materials fabricated by ARB has the striking improvement by comparison with the annealed Cu. This result clearly implies that the ultrahigh strain results in significant strengthening. After 6 ARB cycles, the tensile strength of GNSs/Cu composites is the higher than that of copper. However, the elongation of the ARBed specimen is about 5%, which is typical for SPD/UFG materials [30]. The macroscopic necking after the maximum stress is not so evident compared with the annealed Cu.

Fig. 6 shows that tensile properties of Cu and GNSs/Cu composites vary with the number of ARB cycles. The specimen with the zero number in cycle is the annealed copper used as the raw material. The tensile strength of the ARBed specimens increases with the number of cycles (see Fig. 6a). After 6 ARB cycles, the tensile strength of GNSs/Cu composites reached the maximum value of 496 MPa, which is higher compared to that of the annealed copper by 275 MPa and the ARBed copper by 33 MPa, respectively. Notably, the tensile strength tends to saturate after 6 ARB cycles, and then the strength change is insensitive to the number of cycles. Fig. 6b shows the variation of the elongation with the number of ARB cycles. After 1 ARB cycle, the elongation decreases obviously from 43% for the annealed copper to about 5% for the ARBed specimens. The number of the layers increases accordingly with increasing the ARB cycles. The interfaces act as crack sources and crack propagation during tensile test, which leads to the sharp decrease in elongation. The change trend of the mechanical behavior is similar to experimental results reported in the ARBed copper [31], the ARBed SiC/Cu composites [23] and other SPD/UFG materials [30]. However, after 2 cycles, the increase in the cycle almost does not affect the elongation of the ARBed specimens (keeping about 5%). It is attributed to the increase in the uniform distribution of GNSs in the copper matrix and the sound interfacial bonding in the graphene–copper and copper–copper interfaces during ARB process.

There are two main strengthening mechanisms for the ARBed copper: strain hardening by dislocations and grain refinement [23,31,32]. The tensile strength of the ARBed copper increases

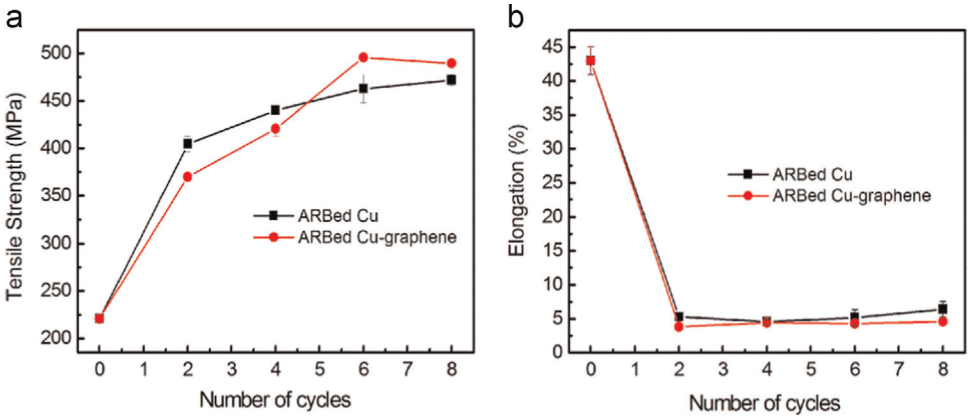

Fig. 6. Variation of tensile strength (a) and elongation (b) with the number of ARB cycles.

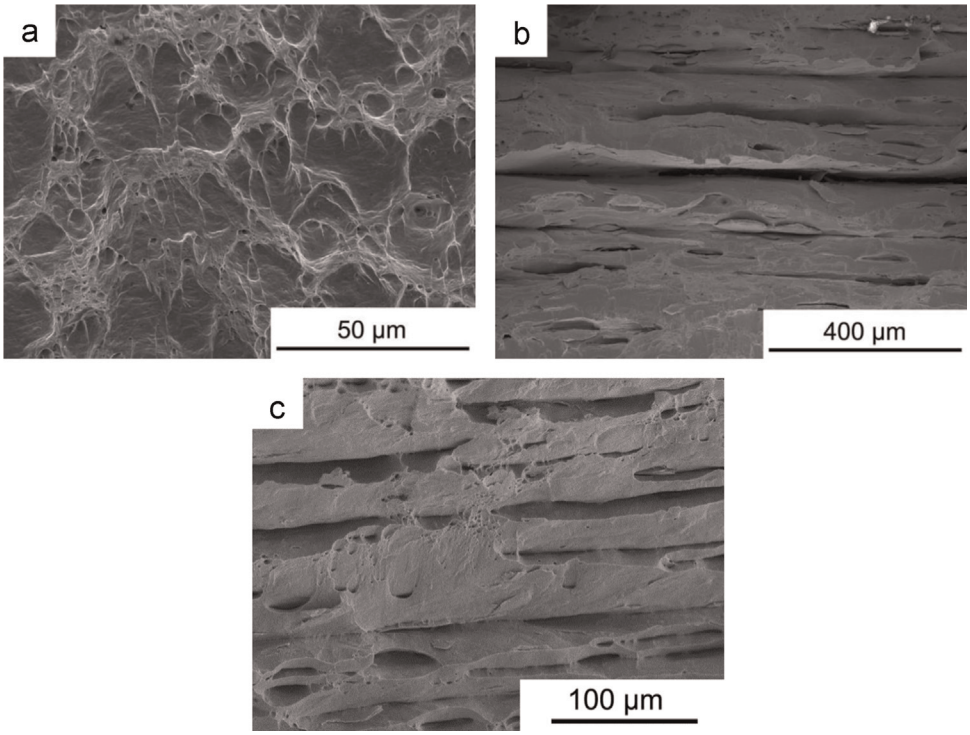

Fig. 7. SEM micrographs of tensile fracture surfaces of the annealed Cu (a), the ARBed Cu (b) and the ARBed GNSs/Cu composites (c) after 6 cycles.

with ARB cycles. Considerable dislocations accumulated at grain boundaries and interfaces provide a significant strain hardening in the ARB process. The contribution of grain refinement to strength matches the Hall–Petch relationship. However, after 6 cycles, the tensile strength of the ARBed GNSs/Cu composites reaches up to 496 MPa, which is slightly higher than that of the ARBed copper. Obviously, GNSs acting as reinforcement plays an important role in strengthening like the second phase ceramic particles in the ARBed GNSs/Cu composites. On the one hand, adding GNSs into the copper matrix leads to an increase in the graphene–copper interfaces, which can effectively impede the dislocation motion and the local plastic deformation. Cu nano-twins are observed near interface of the GNSs/Cu composites, as shown in Fig. 4. For the ARBed Cu, the migration of dislocation can get through from one copper layer to another in the coherent interface [33]. As a result, the GNSs/Cu composites have the higher tensile strength than that for the pure copper at the same ARB cycle. On the other hand, the uniformity of GNSs dispersion and the interface bonding increase gradually with the ARB cycles. These factors benefit to enhance the strength of ARBed composites.

3.2.2. Fractography

Fig. 7 shows the fracture surfaces of the annealed Cu, ARBed Cu and ARBed GNSs/Cu composites after 6 cycles. The fracture surface of the annealed copper has a typical dimple pattern with features of ductile mode of fracture (see Fig. 7a). The Cu and GNSs/Cu composites ARBed for 6 cycles exhibit a mixed-fracture characteristics of few shallow dimples and numerous shear zones, as shown in Fig. 7b and c. The laminated stack structure can be observed and visible cracks appear at the interface between the layers. The necking of the ARBed specimens is not evident in a macroscopic scale, but it can be found within the individual layers in a microscopic scale. Cu layers demonstrate ductile fracture in the ARBed specimens. But the local necking could develop and traverse the whole specimen easily once plasticity instability happens, which results in the elongation deduction.

4. Conclusions

In conclusion, we present an ARB process to fabricate the GNSs/Cu composites with the high strength and ultrafine grain. After 8 ARB cycles, the composites showed a homogeneous dispersion of GNSs and a good interfacial bonding. The addition of GNSs into Cu matrix accelerated the grain refinement. The GNSs/Cu composites formed more UFGs and even NCs. The ARB deformation mechanism is controlled by dislocation motion and twin deformation. The tensile strength of the ARBed GNSs/Cu composites (496 MPa) was the higher than that of the annealed copper (221 MPa) and the ARBed copper (463 MPa), respectively. Except for two main strengthening mechanisms of strain hardening by dislocations and grain refinement, GNSs acting as reinforcement plays a crucial role in strengthening, just like the second phase ceramic particles in the ARBed GNSs/Cu composites. Elongation decreased sharply after the first cycle from 43% to about 5%, but the elongation change was not obvious during ARB. The ARBed Cu and GNSs/Cu composites exhibit mixed-fracture characteristics of few shallow dimples and numerous shear zones.

Acknowledgments

This work was supported by the Natural Science Foundation of Jiangsu Province of China (Grant no. BK20140471), Natural Science Fund for Colleges and Universities in Jiangsu Province of China (Grant no. 12KJB430013) as well as Program for New Century Excellent Talents in University from Chinese Ministry of Education, National Natural Science Foundation of China (Grant nos. 51225102 and 2012CB932203) and the 8th Liuda Rencai Gaofeng (Grant no. B932203) from Jiangsu Province. The authors are grateful to Prof. Wu Zhuangchun for providing graphene nanosheets and thank Prof. Shen Guangjun for TEM analyses.

References

[1] S.R. Allahkaram, S. Golroh, M. Mohammadalipour, Mater. Des. 32 (2011) 4478–4484.
[2] L. Xia, B.B. Jia, J. Zeng, J.C. Xu, Mater. Charact. 60 (2009) 363–369.
[3] P.C. Tsai, Y.R. Jeng, Appl. Surf. Sci. 326 (2015) 131–138.
[4] K. Novoselov, A. Geim, S. Morozov, D. Jiang, Y. Zhang, S. Dubonos, I. Grigorieva, A. Firsov, Science 306 (2004) 666–669.
[5] A.K. Geim, K.S. Novoselov, Nat. Mater. 6 (2007) 183–191.
[6] C. Lee, X. Wei, J.W. Kysar, J. Hone, Science 321 (2008) 385–389.
[7] M. Bastwros, G.Y. Kim, C.N. Zhu, K. Zhang, S.R. Wang, X.D. Tang, X.W. Wang, Composites B 60 (2014) 111–118.
[8] M. Rashad, F.S. Pan, A.T. Tang, M. Asif, M. Aamir, J. Alloy. Compd. 603 (2014) 111–118.
[9] Y.X. Tang, X.M. Yang, R.R. Wang, M.X. Li, Mater. Sci. Eng. A 599 (2014) 247–254.
[10] W. Liu, A. Tkatchenko, M. Scheffler, Acc. Chem. Res. 47 (2014) 3369–3377.
[11] W. Liu, S.N. Filimonov, J. Carrasco, A. Tkatchenko, Nat. Commun. 4 (2013) 2569–2574.
[12] L.Y. Chen, H. Konishi, A. Fehrenbacher, C. Ma, J.Q. Xu, H.S. Choi, H.F. Xu, F. E. Pfefferkorn, X.C. Li, Scr. Mater. 67 (2012) 29–32.
[13] J. Wang, Z. Li, G. Fan, H. Pan, Z. Chen, D. Zhang, Scr. Mater. 66 (2012) 594–598.
[14] D. Kuang, L.Y. Xu, L. Liu, W.B. Hu, Y.T. Wu, Appl. Surf. Sci. 273 (2013) 484–490.
[15] A.N. Sruti, K. Jagannadham, J. Electron. Mater. 39 (2010) 1268–1276.
[16] W.J. Kim, T.J. Lee, S.H. Han, Carbon 69 (2014) 55–65.
[17] M. Alizadeh, M.H. Paydar, D. Terada, N. Tsuji, Mater. Sci. Eng. A 540 (2012) 13–23.
[18] R. Jamaati, S. Amirkhanlou, M.R. Toroghinejad, B. Niroumand, Mater. Sci. Eng. A 528 (2011) 2143–2148.
[19] M. Rezayat, A. Akbarzadeh, Mater. Des. 36 (2012) 874–879.
[20] R. Jamaati, M.R. Toroghinejad, Mater. Sci. Eng. A 527 (2010) 4858–4863.
[21] M. Alizadeh, M. Talebian, Mater. Sci. Eng. A 558 (2012) 331–337.
[22] R. Jamaati, M.R. Toroghinejad, Mater. Sci. Eng. A 527 (2010) 7430–7435.
[23] O. Ghaderi, M.R. Toroghinejad, A. Najafizadeh, Mater. Sci. Eng. A 565 (2013) 243–249.
[24] R. Jamaati, M.R. Toroghinejad, H. Edris, J. Mater. Eng. Perform. 22 (2013) 3348–3356.
[25] R. Jamaati, M.R. Toroghinejad, Mater. Sci. Eng. A 527 (2010) 4146–4151.
[26] C. Lu, K. Tieu, D. Wexler, J. Mater. Process. Technol. 209 (2009) 4830–4834.
[27] C.Y. Liu, Q. Wang, Y.Z. Jia, B. Zhang, R. Jing, M.Z. Ma, Q. Jing, R.P. Liu, Mater. Sci. Eng. A 547 (2012) 120–124.
[28] S.C. Tjong, Mater. Sci. Eng. R 74 (2013) 281–350.
[29] X.R. Liu, Y.B. Liu, X. Ran, J. An, Z.Y. Cao, Mater. Charact. 58 (2007) 504–508.
[30] N. Tsuji, Y. Ito, Y. Saito, Y. Minamino, Scr. Mater. 47 (2002) 893.
[31] M. Eizadjou, A.K. Talachi, H.D. Manesh, H.S. Shahabi, K. Janghorban, Compos. Sci. Technol. 68 (2008) 2003–2009.
[32] R. Jamaati, M.R. Toroghinejad, A. Najafizadeh, Mater. Sci. Eng. A 527 (2010) 2720–2724.
[33] Y.F. Sun, N. Tsuji, H. Fujii, F.S. Li, J. Alloy. Compd. 504 (2010) 443–447.